Synergistic Enhancement of Lung Cancer Therapy Through Nanocarrier-Mediated Sequential Delivery of Superantigen and Tyrosin Kinase Inhibitor

Da Li, Yongbin Li, Haibo Xing, Junling Guo, Yuan Ping, and Guping Tang**

Gefitinib (GFT) and other tyrosine kinase inhibitors (TKIs) have been widely used for the treatment of advanced or metastatic lung cancer due to their reduced side effects when compared to classic cytotoxic chemotherapeutic agents. However, both intrinsic and acquired resistance often hinders the effectiveness of TKIs. Based on recent findings that the outcome of chemotherapy can be influenced by the host immune system at multiple levels, an exploration of whether activating antitumor immunity improves the efficacy of the targeted cancer therapy of TKIs is undertaken. To this end, a cationic carrier is used to deliver superantigen and GFT in a simultaneous or sequential manner. The sequential delivery of superantigen and GFT can significantly enhance T cell immunity, promote cytokine production, inhibit tumor growth, and prolong survival time in tumor models with lung carcinoma xenografts. Most importantly, dual sequential treatment reveals a synergistic effect on tumor inhibition, which is much more effective than the monotherapy of either GFT or pTSA, as well as the combined treatment through simultaneous codelivery of pTSA and GFT together. This study demonstrates the important contribution of immunotherapy to targeted molecular therapy and opens up new possibilities for treating a wide spectrum of cancers.

1. Introduction

Despite recent advances in surgery, chemotherapy and radiation treatment, lung cancer remains one of the leading causes of cancer-related death worldwide. For decades, intravenous cytotoxic chemotherapy, such as platinum-based regimens, has represented the standard first-line treatment for patients with lung cancer.[1] Nevertheless, these cytotoxic drugs generally target both cancer cells and certain normal tissues. As a result, many patients experience the classic toxicities of alopecia, gastrointestinal symptoms, and myelosuppression. During the past ten years, the paradigm for cancer treatment has gradually evolved from relatively nonspecific cytotoxic agents to selective, mechanism-based molecular targeted drugs in an attempt to provide a more effective treatment with fewer side effects. Targeted therapeutic drugs, which typically interfere with a specific molecular target involved in tumor growth and progression, are becoming an important class of therapeutics for breast, colorectal, lung, and pancreatic cancers.[2] Of these molecular drugs, gefitinib (GFT) is known as a tyrosine kinase inhibitor (TKI) and is widely used for the treatment of refractory advanced or metastatic non-small cell lung cancer (NSCLC).[3] GFT inhibits the proliferation of cancer cells by targeting epidermal growth factor receptors (EGFR) that are highly expressed in 80–90% of NSCLC, blocking signal transduction pathways.[4,5] Despite the fact that most NSCLC patients administrated with GFT initially respond to the treatment, they often subsequently experience disease progression while still on the treatment. Different patterns of recurrence were observed after certain periods of survival largely due to mutations in the EGFR or other mutations.[6–8] Several strategies have been proposed to overcome this acquired resistance and enhance the effectiveness of GFT and other EGFR TKIs. Recent strategies include the intensification of EGFR inhibition, the combination of EGFR inhibitors with other targeted therapies, and the use of anticancer therapies acting via alternative pathways.[9,10] Nevertheless, the mechanism of all these proposed modalities remains unclear, and little success has been made to reverse the acquired resistance to TKIs so far. All these facts suggest it is necessary for additional therapies to be developed for improving TKI-based targeted molecular therapy.

Immunotherapy that aims to activate the immune system and enhance antitumor immunity has been recently speculated as a potential modality to consolidate impressive clinical responses from targeted therapies into long-lasting clinical

Dr. D. Li
Department of Medical Oncology
Sir Run Run Shaw Hospital
School of Medicine Zhejiang University
Hangzhou 310016, P.R China
Y. Li, Prof. G. Tang
Institute of Chemical Biology and Pharmaceutical Chemistry
Zhejiang University
Hangzhou 310028, P.R China
E-mail: tangguping@zju.edu.cn
J. Guo, Dr. Y. Ping
Department of Chemical and Biomolecular Engineering
The University of Melbourne
Victoria 3010, Australia
E-mail: yuan.ping@unimelb.edu.au; pingyuan7@gmail.com
Dr. H. Xing
Department of Intensive Care Unit
Sir Run Run Shaw Hospital
School of Medicine Zhejiang University
Hangzhou 310019, P.R China
DOI: 10.1002/adfm.201400456

remissions.[11] Although prospective investigations have not yet been carried out to confirm this hypothesis, there is mounting evidence that cytotoxic chemotherapy outcomes can be influenced by the host immune system at multiple levels. For example, tumor-infiltrating immune effectors were demonstrated to dictate the chemotherapeutic response of breast cancer,[12,13] while the administration of exogenous TNF-α was found to increase the sensitivity of ovarian and other cancer cells to cisplatin and paclitaxel.[14–16] These results imply that cytotoxic chemotherapy may become more effective in immunocompetent hosts than in immunodeficient ones.[17] It is tempting to assume that similar mechanisms might contribute to synergy between targeted molecular therapy and immunotherapy, and activating the immune system is likely to improve the efficacy of targeted cancer therapy.

Superantigens are a class of bacterial and viral proteins that share the ability to activate human and other mammalian T lymphocytes. Bacterial superantigens, such as staphylococcal enterotoxin A (SEA), are potent activators of T cells that can elicit strong immune responses, and induce inflammatory cytokine production and cell-mediated cytotoxicity.[18,19] By fusing the SEA with the transmembrane protein that contains the region sequence encoding the protooncogene c-erb-b2, the resultant transmembrane SEA (TSA) fusion protein was able to effectively anchor to tumor cells, and stimulate the proliferation of lymphocytes in vitro and induce a systemic antitumor immunity in vivo after gene transfection.[20] Furthermore, it was reported that when antibody-superantigen fusion proteins containing SEA were injected into lung tumor-bearing mice, strong antitumor effects were detected, namely high serum levels of IL-2, TNF-α IFN-γ and strong induction of cytotoxic T lymphocytes.[21] These results highlight SEA as a powerful inducer to activate T lymphocytes and produce inflammatory cytokines, meaning SEA may become a complementary therapeutic strategy to targeted molecular therapy by exerting synergistic effects with TKIs. Nevertheless, it remains a great challenge to engineer carriers that are capable of delivering combinational therapeutic agents.

On the basis of these findings, we herein propose a proof-of-concept study for lung cancer therapy through the combinational delivery of TKIs and plasmid DNA encoding TSA protein (pTSA) in an attempt to initiate the synergistic effect of targeted molecular therapy and immunotherapy. Using the cationic polymer 2-hydroxypropyl-β-cyclodextrin-polyethylenimine (HCP) that contains both cyclodextrin (CD) moieties and polyethylenimine (PEI) arms,[22,23] we successfully loaded GFT into the hydrophobic cavity of CD through the formation of a supramolecular inclusion complex (SIC) first. Meanwhile, cationic PEI arms were then used to condense negatively charged pTSA into nanoparticles by electrostatic interactions. Through the combinational delivery of pTSA and GFT into lung cancer cells in either a simultaneous or sequential manner, we expect to demonstrate that enhanced antitumor immunity mediated by pTSA delivery in immunodeficient hosts plays an important role in promoting GFT therapeutic outcomes, and that the combined therapeutic modality is able to cooperatively suppress tumor growth through synergistic effects. To the best of our knowledge, this is the first study to explore how the combination of immunotherapeutic agents and molecular targeted drugs influence overall antitumor effects through carrier-mediated combinational delivery.

2. Results and Discussion

2.1. Carrier Preparation and Cargo Loading

A few types of synthetic vectors such as liposome,[24] cationic micelle,[25–27] dendrimers[28] and mesoporous silica nanoparticles[29] have been recently proposed for the simultaneous loading and delivery of therapeutic genes and anticancer drugs.[30] However, one of the critical issues is to identify a way to simultaneously deliver multiple drugs in a single nanocarrier with the right drug ratios and specific time-programmed release profiles. In addition, the preparation of highly efficient codelivery vectors with low toxicity still represents a great challenge. β-cyclodextrin (β-CD) is well-known for its ability to form complex with a wide spectrum of hydrophobic guest molecules by inclusion in their hydrophobic cavity. β-CD and its derivatives are most widely exploited as solubilizing agents for the hydropholibc small molecule drugs.[31] 2-hydroxylpropyl-β-cyclodextrin (HP-β-CD), a hydroxyalkyl derivative of β-CD, exhibits improved water solubility properties and is well tolerated in humans. On the other hand, low-molecular-weight PEI often shows low toxicity profile but poor transfection activity when compared with 'gold standard' 25 kDa branched PEI. Based on the features of these two building blocks, low-molecular-weight PEI was crosslinked with HP-β-CD through CDI-mediated coupling reaction to obtain HCP that is able to complex plasmid DNA and load GFT in the current study. It is noted to mention that the carbamate linkages, which can be degradable in PBS, ensure the biodegradability of HCP polymer and contribute to reduced cytotoxicity. We have previously demonstrated that HCP-mediated gene transfection efficiency was 1.5–1.7 fold higher than 25 kDa PEI in SKOV-3 (human adenocarcinoma) cell lines, and the similar substitute prepared from 2-hydroxylpropyl-γ-cyclodextrin showed significantly potent anti-tumor effect on SKOV-3 tumor-bearing nude mice in vivo.[22,23] By taking advantage of HP-β-CD's ability to form SICs with guest molecules, GFT was first loaded within the hydrophobic cavity of the HP-β-CD's interior core to form HCP-GFT (**Figure 1**A). The cationic PEI arms surrounding the HP-β-CD were able to further condense pTSA into GFT-loaded, DNA-complexed nanoparticles (Figure 1B). Synthesis of HCP was completed via a one-pot, two-step reaction (Supporting Information, Figure S1). The hydroxyl groups of HP-β-CD were first activated by CDI, and LMW PEI (600 Da) was then crosslinked by the activated HP-β-CD to yield HCP. By mixing GFT with HCP in acidic conditions, GFT could be loaded into the HP-β-CD's cavity of HCP. The ^{1}H NMR spectra of GFT, HCP and HCP-GFT are shown in (Supporting Information, Figure S2). While all the typical proton signals attributed to GFT and HCP were observed, protons from aromatic rings, δ9.9–7.3 ppm, clearly appeared in the case of HCP-GFT, suggesting the GFT was included within the interior core of the HP-β-CD. Two-dimensional nuclear overhauser effect spectroscopy (2D-NOESY) indicated that the proton from 1-chloro-2-fluorobenzene moiety (H_m) was well correlated with the inner

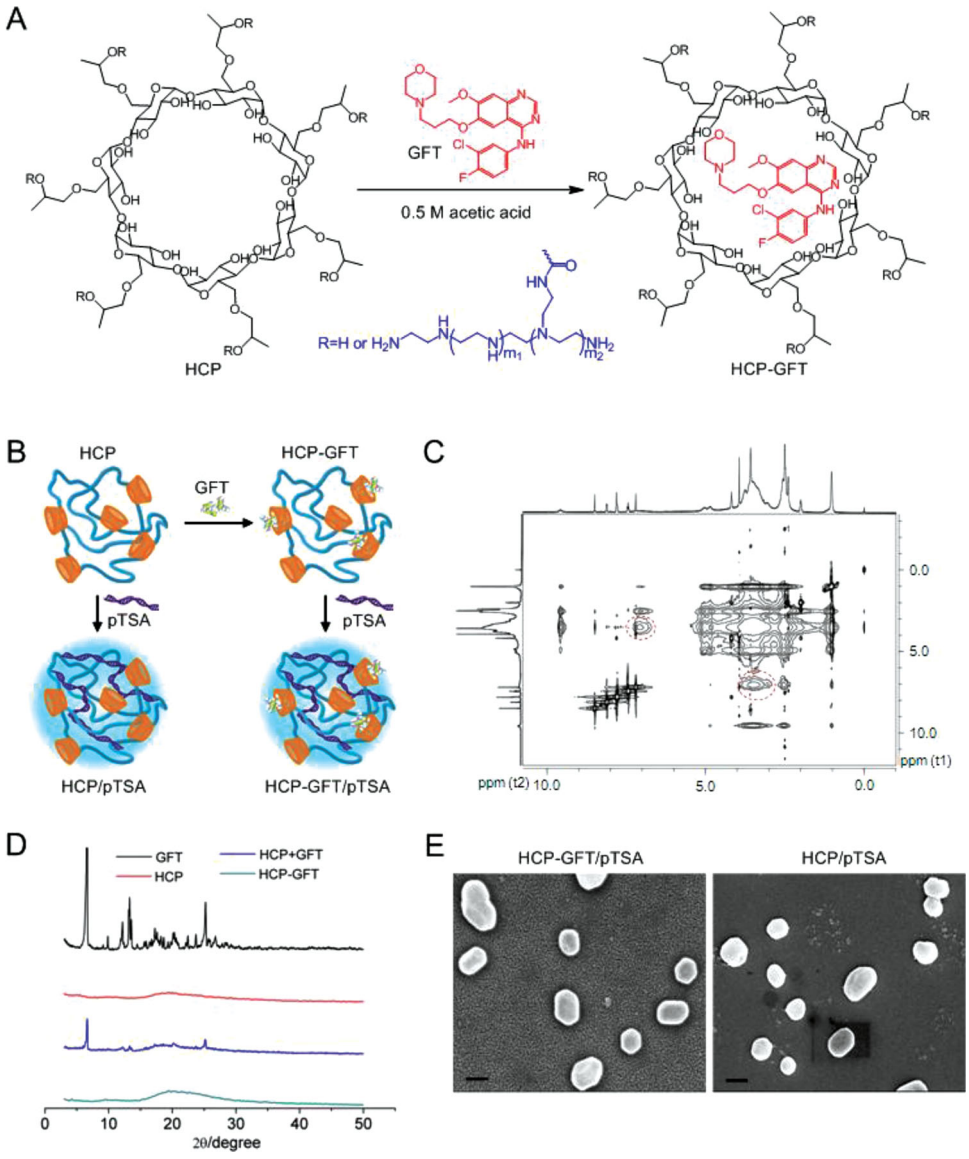

Figure 1. (A) Chemical structure of HP-β-CD-PEI (HCP) and Gefitinib (GFT) as well as HCP-GFT SIC formation between HCP and GFT; (B) Schematic illustration of HCP-GFT SIC formation between HCP and GFT, and the formation of HCP/pTSA complexes and HCP-GFT/pTSA complexes; (C) 2D-NOESY NMR spectrum of HCP-GFT in D_2O; (D) X-ray diffraction analysis of GFT, HCP, HCP-GFT (SICs formed between HCP and GFT) and HCP+GFT (Physical mixture of HCP and GFT); (E) SEM images of HCP/pTSA complexes and HCP-GFT/pTSA complexes. The bars represent 200 nm.

protons of HP-β-CD core, indicating that GFT formed the SIC with the HP-β-CD core (Figure 1C). Moreover, the formation of SICs between HCP and GFT were further confirmed by X-ray diffraction (XRD). Figure 1D shows the XRD patterns of free GFT, HP-β-CD, the physical mixture of HP-β-CD and GFT, and the SIC formed by HP-β-CD and GFT. The sharp reflections from GFT represented the channel-type crystal structure, while the broad peak of HCP represented the amorphous character of the HCP polymers. Meanwhile, when GFT and HCP were physically mixed without the SIC formation, the reflections at $2\theta = 7°$ and 25°, derived from GFT, were clearly observed. However, when GFT formed the SIC with HCP through the host-guest interaction, these reflections from GFT disappeared. This is strong evidence of the amorphous structure of HCP-GFT, suggesting the SIC formation between HCP and GFT. By mixing HCP-GFT with pTSA, the resulting HCPHCP-GFT/pTSA complexes were observed as solid nanoparticles in the range of 100–300 nm under SEM, and there is almost no difference between HCP/pTSA complexes and HCPHCP-GFT/pTSA complexes in term of nanoparticle morphology and size, indicating that loading GFT does not affect the ability of HCP to complex plasmid DNA (Figure 1E). The release kinetics of GFT *in vitro* was also investigated at extracellular physiological pH (7.4) and intracellular endo/lysosomal pH (5.0). At pH 7.4, less than 40% of GFT was released within 36 h, suggesting relative stability at extracellular pH (Supporting Information, Figure S3). In contrast, at a pH of 5.0, fast release was observed within the first five hours, reaching a plateau at 75% released

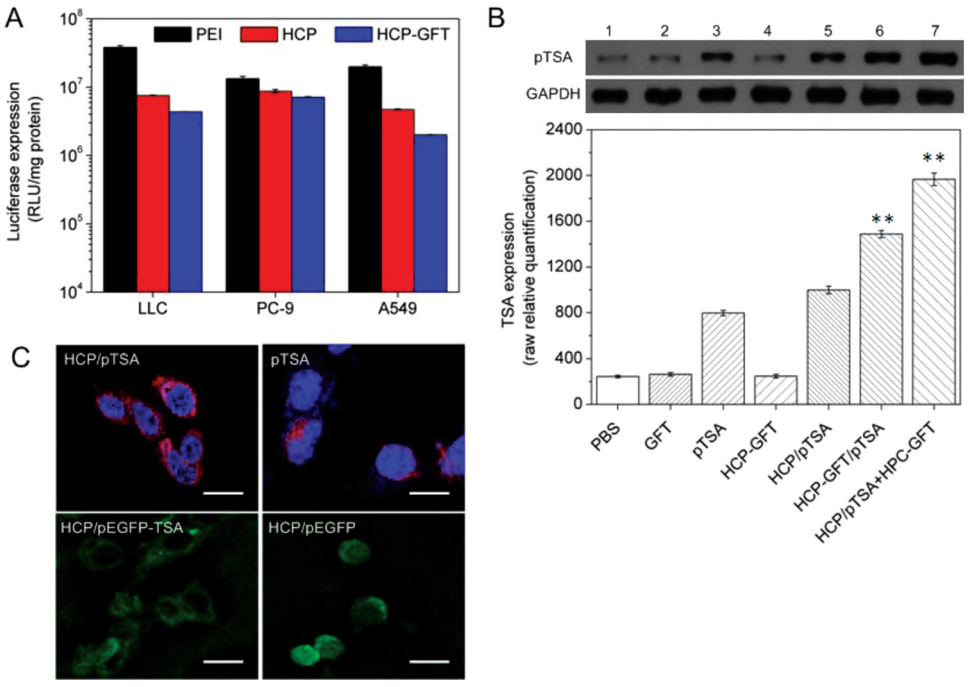

Figure 2. (A) Transfection efficiency HCP and HCP-GFT at the optimal N/P ratio. Luciferase expression was measured at 24 h post-transfection. Data represent mean ± SD (n = 3); (B) Representative TSA protein expression determined by western blot analysis (top). 1, PBS; 2, GFT; 3, pTSA; 4, HCP-GFT; 5, HCP/pTSA; 6, HCP-GFT/pTSA, and 7, HCP/pTSA+HCP-GFT. Quantitative analysis of light intensities of TSA protein expression from western blot results (down). Data represent mean ± SD (n = 3, Student's t-test, **P < 0.01, HCP/pTSA+HCP-GFT vs. HCP-GFT/pTSA, HCP-GFT/pTSA vs. HCP/pTSA or HCP-GFT); (C) Intracellular delivery of HCP/pTSA, pTSA, HCP/pEGFP-TSA and HCP/pEGFP complexes in LLC cells visualized by confocal laser scanning microscope with a standard FITC/TRITC/DAPI filter set. In the upper images (HCP/pTSA and pTSA), the cell nucleus was stained with DAPI (blue), whereas the SEA protein (generated from HCP-mediated pTSA expression) was first treated with mouse anti-SEA primary antibody and then with Alexa Fluor 555-labeled goat anti-Mouse IgG (red). Green fluorescence from the lower images is the result of either pEGFP-TSA expression (lower left) or pEGFP expression (lower right). The scale bar represents 20 μm.

within 12 h. We also found that the complexation of pTSA by HCP-GFT merely affect the GFT release kinetics. It should be also noted that HCP should be stable at 37 °C PBS or serum condition as indicated in our previous similar study.[32] The different release kinetics between extracellular and endocytic pH is probably due to the increased solubility from pH 7.4 to 5.0. When the pH dropped, the enhanced water solubility of GFT would trigger the disassembly of SICs between GFT and the HP-β-CD moiety, leading to the escape of GFT from the hydrophobic cavity of the HP-β-CD. Therefore, the different release kinetics could be applicable to the pH gradient found between the extracellular fluid (pH ~ 7.4) and endosome/lysosome (pH 5.0–6.5), where GFT would be rapidly released at intracellular acidic environments.

2.2. In Vitro Delivery and Cytotoxicity

The transfection activity of HCP and HCP-GFT was evaluated in three types of lung cancer cell lines. Generally, it was found that the transfection efficiency of HCP or HCP-GFT complexes largely depended on the cell type and nitrogen/phosphorus (N/P) ratio (Supporting Information, Figure S4). The optimal N/P ratio that acheived the highest transfection was 35, 35 and 30 in LLC, PC-9 and A549 cells, respectively. At the optimal N/P ratio, HCP showed high transfection activity and reached the same magnitude of luciferase expression as 25 kDa PEI, which is regarded as the 'gold standard' of non-viral vectors (**Figure 2**A). The inclusion of GFT into HCP, however, did not facilitate gene transfection. In fact, HCP-GFT mediated transfection was less efficient when compared with that mediated by HCP alone. Based on these results, we further quantified the TSA protein level derived from the transfection of pTSA in LLC cells through western blot assays. The housekeeping gene, glyceraldehyde 3-phosphate dehydrogenase (GAPDH), was used as a loading control. As indicated in Figure 2B, the transfection of HCP/pTSA complexes resulted in higher levels of gene expression than that of the naked pTSA, suggesting that the cationic HCP polymer could also mediate efficient pTSA transfection. Interestingly, simultaneous codelivery of GFT and pTSA, in which GFT and pTSA were simultaneously loaded and delivered by the same HCP vector (HCP-GFT/pTSA), yielded even higher TSA protein levels than the individual delivery of HCP/pTSA, suggesting that the presence of GFT may promote pTSA gene expression. Sequential delivery of TSA and GFT, in which the HCP/pTSA complexes were first delivered and then HCP-GFT SICs after a period of time (HCP/pTSA+HCP-GFT), resulted in the highest level of gene expression. Although both approaches towards combinational delivery (codelivery and sequential delivery) promoted pTSA expression when compared to the individual delivery of pTSA mediated by HCP, there is a remarkable difference between simultaneous codelivery and

sequential delivery in terms of the level of gene expression. On the basis of above results, we herein propose a potential mechanism of action for the course of pTSA gene expression in the presence of GFT, which could be divided into two relevant but seperate stages. The first stage is pTSA gene expression in the presence of low GFT concentration at the initial GFT release stage, which may promote the pTSA gene expression (termed as 'first stage'). The second stage is the pTSA expression in the presence of high GFT concentration after the first stage due to the large amount of GFT released from HCP, which may impair gene expression as a result of increased cytotoxicity (termed as 'second stage'). For the simultaneous codelivery of pTSA and GFT, the GFT release from HCP may promote gene expression at the first stage but became to slightly inhibit pTSA gene expression at the second stage. For the sequential delivery of pTSA and GFT, pTSA delivery was first carried out in the absence of GFT to reach a high level of gene expression during the first treatment, and the subsequent administration of HCP/GFT would further boost pTSA expression in the first stage. When the local GFT concentration became high at the second stage, pTSA gene expression may already reach the maximum level and the presence of GFT may have minimum negative effect on pTSA gene expression. These results not only suggest that the HCP plays an important role in delivering pTSA efficiently, but also indicates that the presence of GFT may further facilitate pTSA gene expression.

Previous studies showed that the TSA fusion protein possessed the ability to anchor onto living tumor cells due to a hydrophobic transmembrane sequence.[20] In the current study, the ability of the TSA protein to anchor onto the LLC cell membrane was investigated followed by an in-depth look into pTSA gene expression (Figure 2C). When the pTSA delivery was mediated by HCP, strong red fluorescence was observed in the periphery of the cell nucleus due to a high level of pTSA expression, suggesting that the TSA protein did accumulate on the cell membrane. Delivery of naked pTSA, however, yielded a much lower intensity of red fluorescence with the same period of incubation. To further verify gene expression and the location of the TSA protein, we compared the green fluorescence distribution that is generated by means of the transfection of HCP/pEGFP-TSA or HCP/pEGFP complexes in LLC cells (Figure 2C). When the transfection was mediated by HCP/pEGFP-TSA, green fluorescence was mainly distributed on the cellular membrane, making the nuclei area 'hollow'. However, green fluorescence, as a result of HCP-mediated pEGFP gene expression, was observed to distribute evenly inside the cells, which is similar to typical green fluorescence protein expression after carrier-mediated gene transfection.[33] These experiments strongly indicate that the expressed TSA protein possesses a high affinity towards the LLC cell membrane and is able to firmly anchor into the LLC cell membrane.

The cytotoxicities of free GFT, HCP-GFT, and HCP-GFT/pTSA were evaluated as a function of GFT concentration (Supporting Information, Figure S5). Generally, a dose-dependent cytotoxicity was observed with an increased concentration of GFT for all three groups. The HCP-GFT SICs generally exhibited lower cytotoxicity when compared with the equivalent dose of free GFT, which is likely due to cyclodextrin-induced complexation.[31] The effect of SIC formation on reducing GFT cytotoxicity is particularly pronounced in A549 and LLC cells at the GFT concentration ranging from 2 to 8 μM and 2 to 10 μM, respectively. Furthermore, DNA complexation induced by HCP-GFT had little effect on the cytotoxicty profile. HCP/pTSA complexes (without loaded GFT) showed a lower or similar cytotoxicity profile when compared to HCP-GFT/pTSA complexes in terms of the HCP concentration. It is expected that the reduced cytotoxity promotes pTSA expression and facilitates activation of the immune system for anticancer therapy.

2.3. In Vivo T Cell Immunity and Cytokine Production

T cell immunity is the key to protective immune responses against tumors. $CD4^+$ and $CD8^+$ T cells that are identified as providing helper and suppressive effects, respectively, are the main types of lymphocytes involved in T cell-mediated immunity.[34] Therefore, inducing the secretion of circulating tumor-specific T cells in blood promotes antitumor immunity.[35] Moreover, the $CD4^+/CD8^+$ ratio is often considered as an immunobiological indicator for evaluating the status of the immune system in the individual cancer patient.[36] To examine whether there is significant secretion of these T cells, we quantified the serum level of $CD4^+$ and $CD8^+$ T cells using flow cytometry (Supporting Information, Figure S6). As indicated in **Figure 3**A, the $CD4^+$ level decreased slightly when the tumor-bearing mice were administered with HCP/TSA, HCP-GFT/pTSA or HCP/pTSA+HCP-GFT complexes compared with the control groups, and there is no significant increase or decrease in the $CD4^+$ level for the combinational delivery groups. On the other hand, increased $CD8^+$ levels were detected when the tumor-bearing mice were administered with the HCP/pTSA complexes when compared to the HCP-GFT group. Conversely, the administration of HCP-GFT/pTSA did not facilitate $CD8^+$ production and we found that the $CD8^+$ level increased after the mice were sequentially administered the HCP/pTSA+HCP-GFT complexes. The average $CD4^+/CD8^+$ ratio of both HCP/pTSA, HCP-GFT/pTSA and HCP/pTSA+HCP-GFT groups is around 1.5, indicating a relatively healthy status of the tumor-bearing mice after the combined treatments.

Besides T-cell mediated antitumor immunity, cytokines that are released in response to infection, inflammation and immunity can function to inhibit tumor development and progression.[34] Interferon-γ (IFN-γ) signaling in tumor cells plays a role in enhancing tumor immunogenicity, promoting the infiltration of mononuclear cells into the tumor tissue, and inhibiting tumor angiogenesis.[37] Similarly, the tumor necrosis factor-α (TNF-α) was identified for its capacity to induce hemorrhagic necrosis of solid tumors.[38] In this study, IFN-γ and TNF-α were harvested from spleen cells of the tumor-bearing mice and quantified by the enzyme-linked immunosorbent assay (ELISA) (Figure 3B). The TNF-α level significantly increased when the mice were administered with HCP/pTSA or HCP/pTSA+HCP-GFT, when compared to naked TSA or free GFT. Nevertheless, administration of HCP-GFT/pTSA did not promote TNF-α production. Due to the role of TNF-α in sensitizing GFT to lung cancer cells with acquired resistance,[39,40] it is expected that TSA-mediated TNF-α production could alleviate resistance to GFT during lung cancer therapy through the sequential

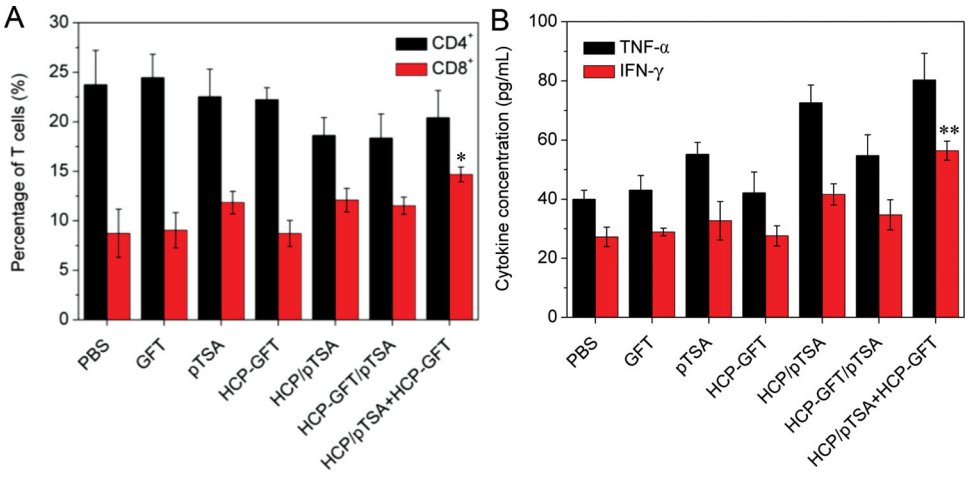

Figure 3. (A) Quantitative analysis of $CD4^+$ and $CD8^+$ cells after intratumoral injection of different formulations in mice. Spleen cells were harvested after successive 3 weeks of administration for flow cytometry analysis (*P<0.05, HCP/pTSA+HCP-GFT vs. HCP-GFT/pTSA or HCP/pTSA); (B) Quantification of cytokines harvested from spleen cells after 3 weeks of successive administration through ELISA assay (**P<0.01, HCP/pTSA+HCP-GFT vs. HCP-GFT/pTSA or HCP/pTSA). All data represent mean ± SD (n = 3).

delivery of HCP/pTSA+HCP-GFT. As for IFN-γ, the administration of HCP/pTSA+HCP-GFT also significantly boosted the IFN-γ level when compared with the administration of either HCP/pTSA or HCP-GFT/pTSA. In the simultaneous codelivery of HCP-GFT/pTSA in vivo, the fast release of GFT owing to the acidity of tumor tissue microenviroment,[41] may impair pTSA expression and therefore affect the production of CD^{8+}, TNF-α and IFN-γ. In the case of sequential delivery of HCP/pTSA+HCP-GFT, HCP/pTSA complexes were first administered, which allows the sufficient production of $CD8^+$, TNF-α or IFN-γ without any interference from GFT. When HCP/GFT complexes were subsequently delivered, the released GFT from HCP may have minimal negative effect on pTSA expression and cytokines and T-cells that were already produced. Collectively, these results not only demonstrate that superantigen-based immunotherapy successfully enhances antitumor immunity, but also suggest that GFT-based targeted cancer therapy may also synergistically modulate immune response in combination with immunotherapy. This last claim is partially supported by a similar study.[42] Therefore, the dual sequential treatment with the HCP/pTSA+HCP-GFT formulation exerted a synergistic effect in activating antitumor immunity, which is expected to promote synergistic tumor suppression.

2.4. In Vivo Antitumor Efficacy of Combined Treatment

Previous study showed that the decrease of EGFR signaling to Akt/NF-nB pathway is directly related to GFT-acquired resistance. As cytokines such as TFN-α could induce autophosphorylation of EGFR, the production of cytokines could sensitize GFT to lung cancer cells with acquired resistance during GFT therapy.[39] Therefore, the administration of superantigen, which facilitates to induce cytokine production in vivo, may reverse the acquired resistance of GFT. On the other hand, the concomitant production of T lymphocytes involved in T cell-mediated immunity could also promote antitumor immunity.[21] Therefore, it is expected that the sequential delivery of superantigen and GFT mediated by HCP may exert a combinational and synergistic effect on the anticancer therapy. In order to assess the therapeutic efficacy of the combined treatment for lung cancer, murine models with LLC xenografts were treated with HCP/pTSA+HCP-GFT or other formulations by intratumoral (i.t.) injection twice a week continuously for 3 weeks (Supporting Information, Figure S7). For dual sequential treatment, different time intervals between the injection of HCP/pTSA and HCP/GFT (12 h, 24 h, 36 h and 48 h) were also optimized, and it was found that the highest level of cytokine and T-cell production was obtained when the time interval was 24 h. As shown in **Figure 4**A, the individual delivery of pTSA or GFT by HCP showed a slight inhibitory effect against tumor growth only after three weeks when compared with PBS treatment, and did not exhibit any greater ability to inhibit tumor growth when compared with the delivery of naked pTSA or free GFT. Combined therapies, on the other hand, generally showed improved antitumor effect compared to monotherapies. As expected, the sequential delivery of pTSA and GFT by HCP exhibited a significant inhibition of tumor growth and was the most effective treatment in inhibiting tumor growth. The average tumor volume from the combined treatments of HCP/pTSA+HCP-GFT was around 650 mm^3, which is much smaller than those observed from the HCP-GFT/pTSA group or other groups (Supporting Information, Figure S8 and Figure S9). Furthermore, the positron emission tomography (PET) imaging, which provides highly sensitive imaging modality for tumor diagnosis, was applied to precisely measure the tumor volume. As shown in Figure 4B, the red color represents the highest intensity. It was clearly shown that the red color area decreased dramatically from monotherapy to combined therapy, which is in agreement with the above results. Almost no red color was observed in the HCP/pTSA+HCP-GFT group from the image, demonstrating that sequential delivery system could substantially inhibit tumor progression. The average weight of dissected tumor from the mice after sequential treatment of HCP/pTSA+HCP-GFT was only around 1.0 g, which is significantly lower than any other group (Figure 4C). It was noted to mention that the

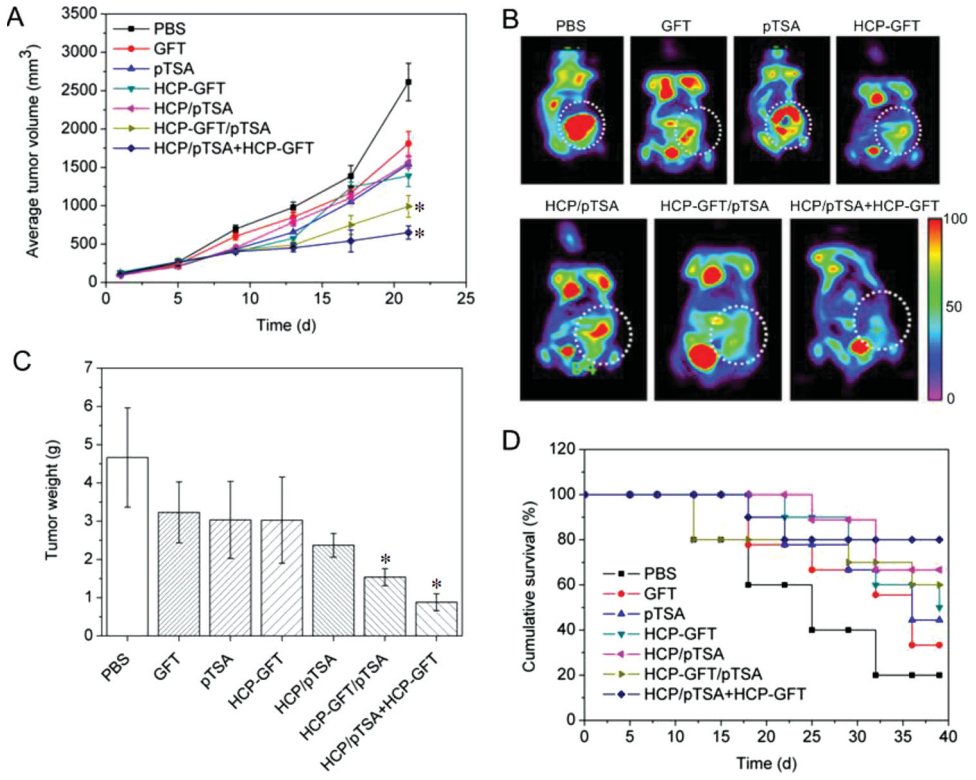

Figure 4. (A) Inhibition of tumor growth in the murine models with LLC xenografts after treatment with various formulations (*P < 0.05, HCP/pTSA+HCP-GFT vs. HCP-GFT/pTSA or HCP/pTSA, HCP-GFT/pTSA vs. HCP/pTSA or HCP-GFT, mean ± SD, n = 3); (B) PET images of in vivo tumor growth 21 days later after first treatments; The intensity is shown by the legend to the lower right; (C) The weight of tumor tissues dissected from mice 21 days later after the first treatment (*P < 0.05, HCP/pTSA+HCP-GFT vs. HCP-GFT/pTSA, HCP-GFT/pTSA vs. HCP/pTSA or HCP-GFT, mean ± SD, n = 3); (D) Survival curves of tumor-bearing mice treated with the different formulations.

mice receiving the treatment of HCP/pTSA+HCP-GFT were found to be most healthy. No ascites was detected after the treatment of 3 weeks, and the mice showed much better appetite and greater flexibility than any other groups. The survival study showed that 80% mice treated with the formulation of HCP/pTSA+HCP-GFT survived the entire 39-day study duration without tumor growth (Figure 4D). The codelivery of pTSA and GFT by HCP was also more efficacious with respect to survival than PBS, free GFT, naked pTSA and HCP-GFT, reaching a survival rate of 60% on the 39th day. These results strongly suggest that the combinational effects of pTSA and GFT through HCP-mediated sequential delivery can substantially inhibited the tumor growth and significantly improve survival in tumor-bearing mice.

During carcinogenesis, tumors develop multiple mechanisms to evade the anti-tumor immune response.[43,44] As found in the current study, the optimal strategy involved dual sequential treatments that first activate the antitumoral immunity by means of superantigen delivery into tumor tissues via i.t. injection. After allowing for sufficient time to activate antitumor immunity in tumor-bearing mice, we continued the second wave of therapy involving i.t. administration of HCP-GFT complexes. It is likely that the enhanced antitumor immunity, which is reflected by up-regulation of superantigen expression, may increase sensitivity of lung cancer cells to GFT. In order to demonstrate that the enhanced tumor suppression by dual sequential delivery of HCP/pTSA+HCP-GFT was related to the up-regulation of TSA protein in the tumor tissues, pTSA gene expression in vivo was evaluated by western blot assay (**Figure 5**). TSA expression was greatly upregulated in tumor-bearing mice after receiving the dual sequential treatment of HCP/pTSA+HCP-GFT and showed highest protein level, which is much higher than codelivery of HCP-GFT/pTSA or individual delivery of HCP/pTSA. Unlike in vitro gene expression, simultaneous codelivery of HCP-GFT/pTSA did not yield higher TSA level when compared with individual delivery of HCP/pTSA. Given the complexity of the in vivo environment, it is difficult to directly correlate in vitro gene expression with in vivo one in terms of simultaneous codelivery. The low level of pTSA expression in the simultaneous codelivery in vivo was probably associated with the acidity of tumor tissue microenvironment,[45,46] which would trigger the fast release of GFT from HCP as compared with in vitro cell culture environment. The high local concentration of GFT may not facilitate pTSA gene expression as discussed earlier. Sequential delivery of HCP/pTSA+HCP-GFT allows the sufficient pTSA expression in the first 24 h without any interference from GFT, and therefore this mode of delivery still shows a high level of pTSA gene expression in vivo. This study strongly suggests the high level of TSA expression is likely to play a crucial role in improving survival time, inhibiting tumor progression and increasing sensitivity of lung cancer cells to GFT.

Cell apoptosis in the tumors after treatment with various formulations were analyzed by the H&E staining and TUNEL assay

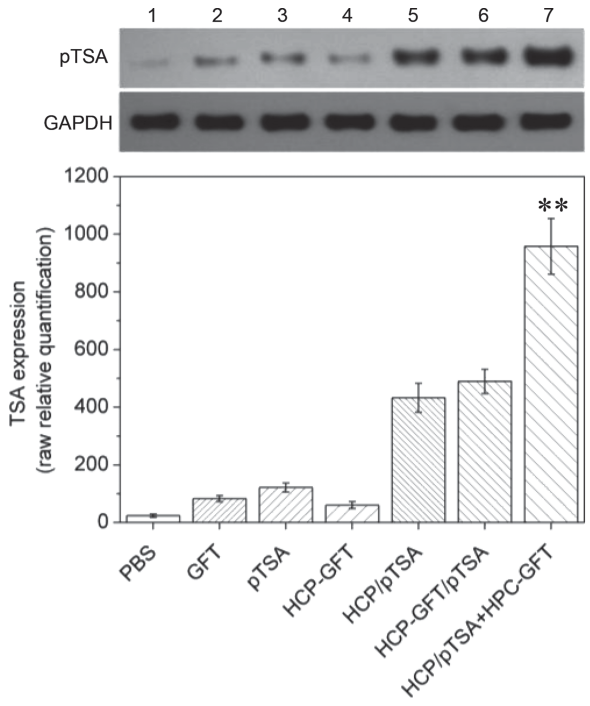

Figure 5. Representative TSA protein expression from tumor tissue determined by western blot analysis (top). 1, PBS; 2, GFT; 3, pTSA; 4, HCP-GFT; 5, HCP/pTSA; 6, HCP-GFT/pTSA, and 7, HCP/pTSA+HCP-GFT. Quantitative analysis of light intensities of in vivo TSA protein expression from western blot results (down, **P < 0.01, HCP/pTSA+HCP-GFT vs. HCP-GFT/pTSA or HCP-GFT/pTSA). All quantitative data represent mean ± SD (n = 3).

(**Figure 6**). The H&E stained sections of tumor tissues from the PBS and pTSA control groups appeared most hypercellular and showed more obviously the nuclear polymorphism. Among the five therapeutic groups, the tumor tissues from the treatments with the formulation of HCP/pTSA+HCP-GFT showed the fewest tumor cells and the highest level of tumor necrosis. The TUNEL assay also showed that the combined sequential treatment with the formulation of HCP/pTSA+HCP-GFT can induce much more TUNEL-positive cells. These results further validate the effectiveness of the combined treatment through the sequential delivery of pTSA and GFT with HCP.

3. Conclusions

We have successfully established a new therapeutic modality that combines immunotherapy and targeted molecular therapy for the effective treatment of lung cancer through the carrier-mediated combinational delivery of superantigens and TKIs. This modality combines the advantages of superantigens to activate antitumor immunity with the specificity feature of TKIs to selectively induce tumor cell apoptosis. The sequential delivery of HCP/pTSA+HCP-GFT complexes greatly upregulated the TSA protein level in tumor tissues, enhanced T cell immunity, and promoted cytokine production in tumor-bear mice. Most importantly, the sequential delivery of HCP/pTSA+HCP-GFT substantially inhibited the tumor growth and effectively prolong suvival time in vivo, which is most likely related to the high level of pTSA gene expression that enhanced the antitumor immunity in tumor-bearing mice. The current study also highlights the sequence for delivering immunotherapeutic agents and targeted drugs greatly influence the overall antitumor effects of the combined treatment. The success of this combinational modality not only defines a unique strategy for effective lung cancer therapy, but also opens up new possibilities for treating a wide spectrum of cancers in the dawning era of personalized nanomedicine.

4. Materials and Methods

Materials: (2-Hydroxypropyl)-β-cyclodextrin, polyethyleneimine (branched PEI, molecular weight 600 Da and 25 K Da), 1,1′-carbonyldiimidazole(CDI), [3-(4,5-dimethylthiazol-2-yl)-2,5-diphenyltetrazolium bromide] (MTT), triethylamine (Et_3N) were purchased from Sigma-Aldrich (USA). GFT (GFT) was purchased from Hangzhou Hexo Chemtech Co. Ltd. 2-(4-amidinophenyl)-6-indolecarbamidine dihydrochloride (DAPI), antifade mounting medium, Alexa Fluor 555-labeled Goat Anti-Mouse IgG (H+L) were purchased from Life technologies (Grand Island, USA). Staphylococcus aureus Enterotoxin A (SEA) antibody was obtained from GeneTex Inc (Irvine, USA). PE Rat Anti-Mouse $CD4^+$ and PE Rat Anti-Mouse $CD8^+$ were purchased from QuantoBio Inc (Beijing, China). Mouse α-TNF and γ-IFN ELISA Kit was purchased from Boster (Pleasanton, USA). Plasmid pGL3 encoding firefly luciferase was purchased from Promega (Madison, USA). Plasmid TSA encoding transmembrane-staphylococcal enterotoxin A protein, and plasmid EGFP-TSA encoding green fluorescence protein fused with transmembrane-staphylococcal enterotoxin A protein were synthesized by Hangzhou Hebei Scientific Co. Ltd. (Hangzhou, China).

Cell Culture: All cell lines used in this study were purchased from ATCC. Human lung adenocarcinoma cell line PC-9 was cultured in Dulbecco's Modified Eagle's Medium (DMEM) supplemented with 10% calf serum (CS). Human lung carcinoma cell line A549 was cultures in RPMI 1640 culture medium supplemented with 10% CS. Lewis lung cancer (LLC) cells in mice was cultured in Dulbecco's Modified Eagle's Medium (DMEM) supplemented with 10% fetal bovine serum (FBS). Cells were cultured at 37 °C in humidified atmosphere containing 5% CO_2.

General Characterization: The ^1H and 2D-NOESY NMR spectra of each sample were acquired on a Bruker DRX-400 spectrometer (Bruker, Ettlingen, Germany) at room temperature using either deuterium oxide (D_2O) or dimethyl sulfoxide-d_6 (DMSO-d_6) as the solvent. The morphology of the complexes was examined by field-emission scanning electron microscopy (FE-SEM, JEOL JSM-7400F, Japan). X-ray diffraction (XRD) was performed on a Rigaku D/max 2550PC diffractometer System (Japan) with Cu Kα radiation.

Synthesis of HCP-GFT: HCP was first prepared according to our previous method.[22] To prepare HCP-GFT SICs, HCP (230 mg) was dissolved in 15 mL of 0.5 M acetic acid solution, and then GFT (39 mg, 0.087 mmol) was dissolved in another 10 mL of 0.5 M acetic acid solution. After both substances completely dissolved, the two solutions were mixed and stirred for 5 min. The aqueous solution was then frozen at −20 °C and freeze-dried for approximately 48 h. The final product HCP-GFT was obtained as a light yellow solid.

Preparation of GFT-loaded, pDNA-complexed Nanoparticles: Plasmid DNA (pGL3, pTSA or pTSA-EGFP) was diluted to a concentration of 0.2 mg/mL. An appropriate amount of HCP-GFT was added into DNA solution and the solution mixture was mixed using a vortexer. The solution was incubated at room temperature for 20 min before use.

Release of GFT from HCP-GFT: To quantitatively determine the release of GFT, HCP-GFT (2 mg) in 50 mL of acetate buffer solutions (pH = 5.0) or phosphate-buffered saline (PBS) buffer (pH = 7.4) were incubated at 37 °C in dialysis bags in solutions with mild stirring. At

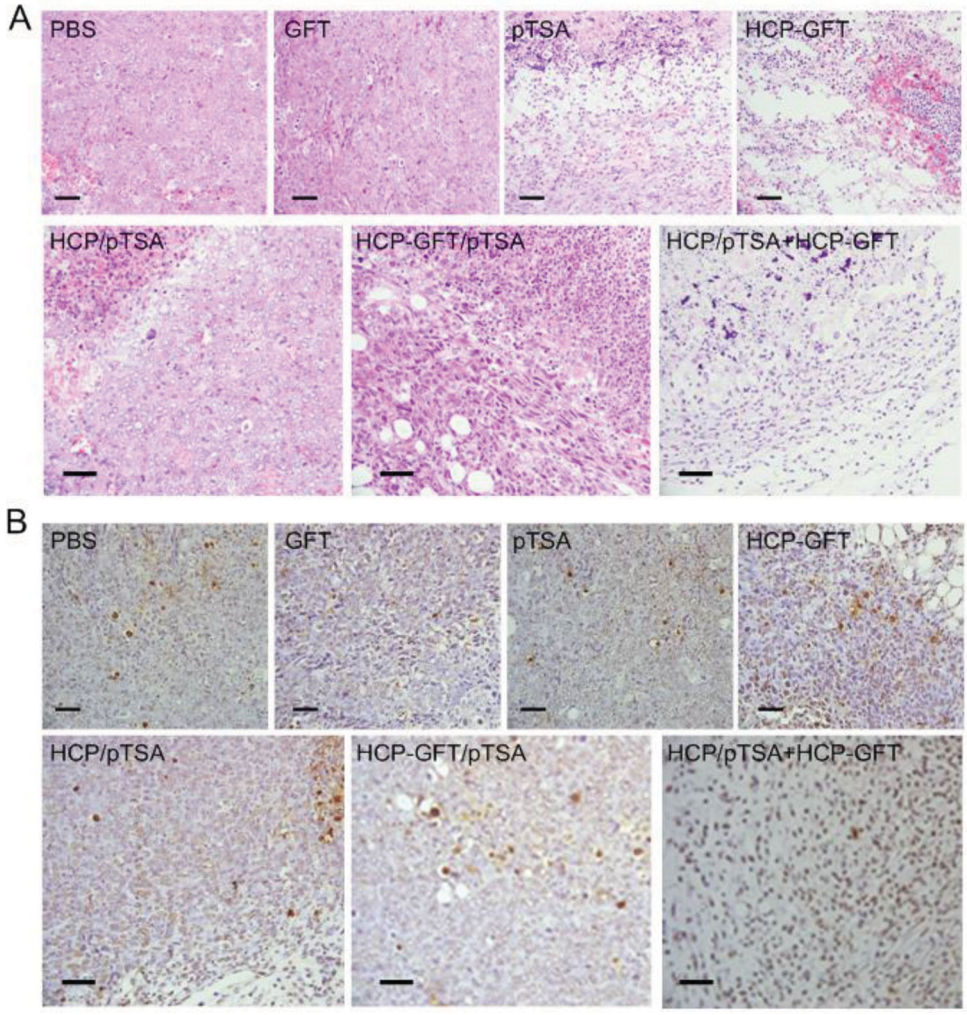

Figure 6. H&E staining (A) and TUNEL assay (B) of tumor tissues treated with different formulations. Scale bars represent 20 μm.

predefined time points, 1.0 mL of the sample was collected from the solution outside the dialysis bags. The UV absorbance was measured on a UV Spectrophotometer (UV-3600, Shimazu, Japan) at the wavelength of 252 nm. The GFT concentration was calculated with a standard curve calibrated with GFT samples of known concentration. The GFT concentration in the solution was calculated based on the standard curve calibrated with GFT solutions of known concentrations.

Cell Viability Assay: MTT method was used to evaluate cell viability assay according to the previous method.[47] The A549, PC-9 and LLC cells were seeded at 1×10^4 cells/well in 200 μL serum-containing medium in 96-well plates. After 24 h, the medium was replaced by fresh medium containing various concentrations of free GFT, HCP-GFT or HCP-GFT/pTSA complexes. After incubation 24 h, 10 μL of 5 mg/mL filtered MTT stock solution was added to each well, and unreacted dye was removed by aspiration after 4 h. The formazan crystals were dissolved in 100 μL per well DMSO and were measured on a microplate reader (Model 680, Bio-Rad) at the wavelength of 570 nm. The cell viability was expressed as a relative percentage of the untreated cells.

In Vitro Gene Transfection: The luciferase expression mediated by HCP/pGL3 and HCP-GFT/pGL3 complexes was evaluated using A549, PC-9 and LLC cell lines according to the reported protocol.[48] Cells were seeded in 48-well plates at a density of 2×10^4 cells/well and incubated for 18 h. The medium was replaced with 500 μL of fresh serum-free DMEM medium containing complexes with 1 μg pGL3 at different N/P ratios. After 4 h incubation, the transfection media were replaced with complete medium and incubated for another 48 h. Luciferase activity was measured according to standard protocols of luciferase assay system (Promega, USA). The total protein was measured according to a BCA protein assay kit (Pierce, USA) and luciferase activity was reported in terms of RLU/mg cellular protein. For pTSA gene transfection, LLC cells were seeded in 24-well plates at a density of 3×10^4 cells per well in 800 μL of complete DMEM culture media and incubated for 18 h. Then the original cell culture media were replaced with the polyplex solution containing 1 μg pTSA at the N/P ratio of 30 in 500 μL serum-free DMEM culture media for each well. After 4 h incubation, the transfection media were replaced with complete medium and incubated for 44 h. In case of HCP/pTSA+HCP-GFT group, the HCP/pTSA complexes were incubated with the medium for 4 h first and were then replaced with complete medium to culture the cells for 20 h. Afterwards, HCP-GFT complexes were then added and incubated in the medium for 4 h first, and were replaced with complete medium to culture the cells for another 44 h. The cells were washed with PBS for 3 times followed by fixation with 10% formaldehyde solution for 10 min. Fixed cells were blocked with 1% BSA for 20 min. After washing with PBS, the cells were incubated for 90 min with SEA antibody diluted 500 times with PBS. After a further wash in PBS, the cells were incubated with Alexa Fluor 555-labeled Goat Anti-Mouse IgG according to the manufacturers' suggestion. DAPI was used to stain cell nuclei for 10 min. Labeled cells were visualized by

confocal laser scanning microscopy (CLSM) using a Zeiss LSM 510 laser scanning microscope (Carl Zeiss, Germany).

Western Blot Analysis: For western blotting analysis, the cells were transfected as described above and the cell proteins were extracted after 48 h of transfection. The total protein was quantified by the BCA protein assay kit (Promega, USA). The equal amount of protein was separated on the SDS-PAGE, transferred onto nitro-cellulose membrane, blocked and incubated overnight with monoclonal antibodies against SEA (1:500). After washing, the membrane was incubated with horseradish peroxidase -conjugated secondary antibody (1:5000) for 2 h at room temperature. The bands were visualized using the Westzol enhanced chemiluminescence detection kit (Intron, Korea) and the expression was normalized with housekeeping gene expression.

Establishment of Animal Tumor Models: Animal experiments were performed in accordance with the regulations of China Animal Protection Network, and all protocols used in the study were approved by the Zhejiang University Animal Care and Use Committee. C57BL/6 female mice (4–6 weeks, 18–22 g weight) were purchased from Zhejiang University Animal Care Center and maintained in a pathogen-free environment under controlled temperature (24 °C). LLC cells were transplanted into the left abdominal of the mices to establish the tumor models.

In Vivo Antitumor Activity and Histological Assay: LLC cells were injected subcutaneously (0.1 mL injection volume; 1×10^6 cells) at the left abdominal of C57BL/6 mice. When tumor grew to a diameter of 4–6 mm within 10 days, the mice were randomly assigned to 7 groups (8 mice for each group). Normal saline, GFT, naked pTSA, HCP-GFT, HCP/pTSA and HCP-GET/pTSA at an equivalent dose of 35 μg GFT and 30 μg pTSA in a total volume of 100 μL were administrated via i.t. injection, respectively. For HCP/pTSA+HCP-GFT group, the mice were first injected with HCP/pTSA containing 30 μg pTSA, and were then injected HCP-GFT SICs containing 35 μg GFT after 24 h. The treatments were performed twice a week for continuous 3 weeks. The tumor growth was monitored by measuring tumor length (l) and width (w) with a caliper. The tumor volume was calculated as $V = \pi/2 \times lw^2$. Three mice from each group were sacrificed 3 weeks later after the first injection. The tumors were dissected, weighed, and then imaged.

In Vivo Positron Emission Tomography (PET) Imaging: 18F-fluorodeoxyglucose (18F-FDG) micro PET imaging was performed on a microPET R4 scanner (Concorde Microsystems, Knoxville, TN, USA) which consisted of a 15-cm diameter ring of 96 position-sensitive γ-ray scintillation detectors, providing a 10-cm transaxial and a 7-cm axialfield of view with an image resolution of <1.8 mm. The transaxial image planes were separated by 1.2 mm. In brief, 1.5 min halothane gas anesthesia was performed and the mice were intravenously injected with 500mCi/mmol 18F-FDG via the dorsal penile vein. Then, the mice were caged again and placed in a room with minimal ambient noise. They were allowed to move around for 40 min after tracer injection. Subsequently, the animals were placed in the microPET scanner under halothane gas anesthesia (5% induction and 1.5% for maintenance). A 15-min static acquisition was performed in 3D mode.

Histological Analysis and TUNEL Assay: For the histological assay, the tumor tissues were fixed in 4% paraformaldehyde for 24h. The specimens were then dehydrated in graded ethanol, embedded in paraffin, and cut into 5-mm-thick sections. The fixed sections were deparaffinized and hydrated according to a standard protocol and stained with hematoxylin and eosin (H&E) for microscopic observation. The apoptosis of tumor cells following treatments in the mice was determined using the TUNEL method according to the manufacturer's instructions (Roche, Basel, Switzerland). All sections were examined on a Leica (DMLB&DMIL) microscope.

In Vivo IFN-γ and TNF-α Quantification: Spleens from three mice per group were removed aseptically 3 weeks following immunization and washed twice in PBS solution. The spleens were crushed by 200 mesh nylon net and splenocytes were suspended in 5 mL EZ-Sep mouse 1× lymphocyte separation medium (Eton bioscience Inc, USA). This single-cell suspension was added to 500 μL RPMI 1640 medium and centrifuged for 30 min at 800 g. Cells from the intermediate layer were collected, washed three times with fresh RPMI 1640 and then centrifuged for 10 min at 250 g. The splenocytes were collected and suspended in 5 mL RPMI 1640 culture medium supplemented with 10% CS for 24 h. Supernatants were collected and cytokines were quantified using Mouse TNF-α ELISA Kit and IFN-γ Mouse ELISA Kit (Life technologies, USA).

In Vivo $CD8^+$ and $CD4^+$ T Cell Analysis: Spleen cells were resuspended in PBS at 2×10^7/mL, and was added with 1% BSA in PBS to block nonspecific labeling due to FcR binding. Cells were then incubated with phycoerythrin-conjugated mouse anti-rat CD8a or CD4 monoclonal antibody (1.0 μg/10^6 cells) for 1 h in the dark to label T cells. The cells were washed and a minimum of 10 000 cells were analyzed in each sample using an EPICS XL flow cytometer (Beckman-Coulter, USA).

Statistical Analysis: All experiments were repeated at least three times. Data are presented as mean ± standard deviation. Statistical significance was evaluated by using Student t-test when two groups were compared.

Supporting Information

Supporting Information is available from the Wiley Online Library or from the author.

Acknowledgments

D.L. and Y.L. contributed equally to this work. D.L, Y.L., Y.P., and G.T. designed research; D.L., Y.L., and Y.P. performed research; Y.L. J.G., and Y.P. analyzed data; H.X. contributed new reagents/analytic tools; and Y.L. and Y.P. wrote the paper. This work was jointly supported by Chinese National Natural Science Foundation (No. 21374098 & No. 81001034) and Research Foundation for Health and Medical Sciences of Zhejiang Province (No. 2009B087).

Received: February 10, 2014
Revised: March 13, 2014
Published online: June 20, 2014

[1] J. R. Molina, P. Yang, S. D. Cassivi, S. E. Schild, A. A. Adjei, *Mayo Clin. Proc.* **2008**, *83*, 584.
[2] C. Sawyers, *Nature* **2004**, *432*, 294.
[3] R. Govindan, R. Natale, J. Wade, R. Herbst, A. Krebs, R. Reiling, T. Hensing, A. Wozniak, C. P. Belani, K. Kelly, J. Ochs, *Lung Cancer* **2006**, *53*, 331.
[4] K. Tamura, M. Fukuoka, *Expert Opin. Pharmacother.* **2005**, *6*, 985.
[5] V. Rusch, J. Baselga, C. Cordon-Cardo, J. Orazem, M. Zaman, S. Hoda, J. McIntosh, J. Kurie, E. Dmitrovsky, *Cancer Res.* **1993**, *53*, 2379.
[6] W. Pao, T. Y. Wang, G. J. Riely, V. A. Miller, Q. Pan, M. Ladanyi, M. F. Zakowski, R. T. Heelan, M. G. Kris, H. E. Varmus, *PLoS Med.* **2005**, *2*, e17.
[7] S. Kobayashi, T. J. Boggon, T. Dayaram, P. A. Janne, O. Kocher, M. Meyerson, B. E. Johnson, M. J. Eck, D. G. Tenen, B. Halmos, *N. Engl. J. Med.* **2005**, *352*, 786.
[8] E. L. Kwak, R. Sordella, D. W. Bell, N. Godin-Heymann, R. A. Okimoto, B. W. Brannigan, P. L. Harris, D. R. Driscoll, P. Fidias, T. J. Lynch, S. K. Rabindran, J. P. McGinnis, A. Wissner, S. V. Sharma, K. J. Isselbacher, J. Settleman, D. A. Haber, *Proc. Natl. Acad. Sci. USA* **2005**, *102*, 7665.
[9] G. R. Oxnard, M. E. Arcila, J. Chmielecki, M. Ladanyi, V. A. Miller, W. Pao, *Clin. Cancer Res.* **2011**, *17*, 5530.
[10] G. R. Oxnard, *Arch. Pathol. Lab. Med.* **2012**, *136*, 1205.
[11] M. Vanneman, G. Dranoff, *Nat. Rev. Cancer* **2012**, *12*, 237.
[12] C. Denkert, S. Loibl, A. Noske, M. Roller, B. M. Müller, M. Komor, J. Budczies, S. Darb-Esfahani, R. Kronenwett, C. Hanusch,

C. von Törne, W. Weichert, K. Engels, C. Solbach, I. Schrader, M. Dietel, G. von Minckwitz, *J. Clin. Oncol.* **2010**, *28*, 105.
[13] H. Hornychova, B. Melichar, M. Tomsova, J. Mergancova, H. Urminska, A. Ryska, *Cancer Invest.* **2008**, *26*, 1024.
[14] R. Uslu, B. Bonavida, *Cancer* **1996**, *77*, 725.
[15] A. Sacchi, A. Gasparri, C. Gallo-Stampino, S. Toma, F. Curnis, A. Corti, *Clin. Cancer Res.* **2006**, *12*, 175.
[16] A. Bamias, V. Koutsoukou, E. Terpos, M. L. Tsiatas, C. Liakos, O. Tsitsilonis, A. Rodolakis, Z. Voulgaris, G. Vlahos, T. Papageorgiou, G. Papatheodoridis, A. Archimandritis, A. Antsaklis, M. A. Dimopoulos, *Gynecol. Oncol.* **2008**, *108*, 421.
[17] L. Zitvogel, O. Kepp, G. Kroemer, *Nat. Rev. Clin. Oncol.* **2011**, *8*, 151.
[18] M. Dohlsten, A. Sundstedt, M. Bjorklund, G. Hedlund, T. Kalland, *Int. J. Cancer* **1993**, *54*, 482.
[19] M. Dohlsten, P. A. Lando, G. Hedlund, J. Trowsdale, T. Kalland, *Immunology* **1990**, *71*, 96.
[20] W. Ma, H. Yu, Q. Wang, J. Bao, J. Yan, H. Jin, *Cancer Immunol. Immunother.* **2004**, *53*, 118.
[21] A. Rosendahl, J. Hansson, A. Sundstedt, T. Kalland, M. Dohlsten, *Int. J. Cancer* **1996**, *68*, 109.
[22] H. L. Huang, G. P. Tang, Q. Q. Wang, D. Li, F. P. Shen, J. Zhou, H. Yu, *Chem. Commun.* **2006**, 2382.
[23] H. L. Huang, H. Yu, G. P. Tang, Q. Q. Wang, J. Li, *Biomaterials* **2010**, *31*, 1830.
[24] W. Xiao, X. Chen, L. Yang, Y. Mao, Y. Wei, L. Chen, *Int. J. Pharm.* **2010**, *393*, 119.
[25] H. Y. Huang, W. T. Kuo, M. J. Chou, Y. Y. Huang, *J. Biomed. Mater. Res. A* **2011**, *97*, 330.
[26] C. H. Zhu, S. Jung, S. B. Luo, F. H. Meng, X. L. Zhu, T. G. Park, Z. Y. Zhong, *Biomaterials* **2010**, *31*, 2408.
[27] A. L. Lee, Y. Wang, H. Y. Cheng, S. Pervaiz, Y. Y. Yang, *Biomaterials* **2009**, *30*, 919.
[28] Y. Ren, C. S. Kang, X. B. Yuan, X. Zhou, P. Xu, L. Han, G. X. Wang, Z. Jia, Y. Zhong, S. Yu, J. Sheng, P. Y. Pu, *J. Biomat. Sci. Polym. Ed.* **2010**, *21*, 303.
[29] A. M. Chen, M. Zhang, D. Wei, D. Stueber, O. Taratula, T. Minko, H. He, *Small* **2009**, *5*, 2673.
[30] N. N. Choudhury, H. He, *Curr. Pharm. Biotechnol.* **2012**, *13*, 1317.
[31] M. E. Davis, M. E. Brewster, *Nat. Rev. Drug Discov.* **2004**, *3*, 1023.
[32] G. P. Tang, H. Y. Guo, F. Alexis, X. Wang, S. Zeng, T. M. Lim, J. Ding, Y. Y. Yang, S. Wang, *J. Gene Med.* **2006**, *8*, 736.
[33] Y. Ping, C. D. Liu, Z. X. Zhang, K. L. Liu, J. H. Chen, J. Li, *Biomaterials* **2011**, *32*, 8328.
[34] G. Dranoff, *Nat. Rev. Cancer* **2004**, *4*, 11.
[35] A. Bolhassani, F. Zahedifard, *Int. J. Cancer* **2012**, *131*, 1733.
[36] F. Brivio, L. Fumagalli, D. Parolini, G. Messina, F. Rovelli, R. Rescaldani, L. Vigore, R. Vezzo, M. Vaghi, S. Di Bella, P. Lissoni, *In Vivo* **2008**, *22*, 647.
[37] G. L. Beatty, Y. Paterson, *Immunol. Res.* **2001**, *24*, 201.
[38] E. A. Carswell, L. J. Old, R. L. Kassel, S. Green, N. Fiore, B. Williamson, *Proc. Natl. Acad. Sci. USA* **1975**, *72*, 3666.
[39] K. Ando, T. Ohmori, F. Inoue, T. Kadofuku, T. Hosaka, H. Ishida, T. Shirai, K. Okuda, T. Hirose, N. Horichi, K. Nishio, N. Saijo, M. Adachi, T. Kuroki, *Clin. Cancer Res.* **2005**, *11*, 8872.
[40] Y. Ji, S. L. Ma, Y. P. Zhang, J. J. Tang, Y. M. Wu, Y. J. Lu, *Anticancer Drugs* **2009**, *20*, 832.
[41] I. F. Tannock, D. Rotin, *Cancer Res.* **1989**, *49*, 4373.
[42] V. P. Balachandran, M. J. Cavnar, S. Zeng, Z. M. Bamboat, L. M. Ocuin, H. Obaid, E. C. Sorenson, R. Popow, C. Ariyan, F. Rossi, P. Besmer, T. Guo, C. R. Antonescu, T. Taguchi, J. Yuan, J. D. Wolchok, J. P. Allison, R. P. DeMatteo, *Nat. Med.* **2011**, *17*, 1094.
[43] M. Ahmad, R. C. Rees, S. A. Ali, *Cancer Immunol. Immunother.* **2004**, *53*, 844.
[44] F. H. Igney, P. H. Krammer, *J. Leukoc. Biol.* **2002**, *71*, 907.
[45] L. E. Gerweck, K. Seetharaman, *Cancer Res.* **1996**, *56*, 1194.
[46] K. Engin, D. B. Leeper, J. R. Cater, A. J. Thistlethwaite, L. Tupchong, J. D. McFarlane, *Int. J. Hyperthermia* **1995**, *11*, 211.
[47] Y. Ping, C. D. Liu, G. P. Tang, J. S. Li, J. Li, W. T. Yang, F. J. Xu, *Adv. Funct. Mater.* **2010**, *20*, 3106.
[48] Y. Ping, Q. Hu, G. Tang, J. Li, *Biomaterials* **2013**, *34*, 6482.